Glass-Based Bandpass Filters for New Radio (NR) *K*-/*Ka*-Band Communications

Dimitra Psychogiou, *Senior Member, IEEE*, and Andrea Ashley, *Graduate Student Member, IEEE*

***Abstract*— Highly miniaturized substrate integrated coaxial (SIC) bandpass filters (BPFs) are presented for new radio (NR) communications. They are based on glass-integrated two-post SIC resonators and mixed electromagnetic (EM) couplings that contribute to two poles and one transmission zero (TZ) to the overall BPF transfer function. The concept can be extended to high-order quasi-elliptic configurations shaped by $2N$ poles and N TZs by readily cascading N two-post SIC cavities through inter-stage transmission lines (TLs). A high-frequency glass-based integration platform is explored as a low-loss and high-frequency integration mechanism. To practically validate the concept, three glass-integrated BPF prototypes were designed, manufactured, and tested. They include a: 1) two-pole/one-TZ BPF with a passband centered at 26 GHz, fractional bandwidth (FBW) of 21%, and a TZ at 32 GHz; 2) two-pole/one-TZ BPF with a passband centered at 26.7 GHz, FBW of 11%, and a TZ at 23.6 GHz; and 3) a four-pole/two-TZ BPF with a passband centered at 26.7 GHz, FBW of 11%, and two TZs at 24 and 31.3 GHz.**

***Index Terms*— Bandpass filter (BPF), coaxial filter, compact filter, millimeter-wave filter, substrate integrated filter.**

I. Introduction

NEXT-GENERATION wireless communications will leverage frequency bands in the high-frequency range of the spectrum to achieve higher data rates and smaller form factor devices than what is currently possible in sub-6 GHz bands. In particular, the recently licensed frequency bands (*n*257, 258, 261) within the *K*-/*Ka*-band are creating new opportunities for 5G communications through the realization of terrestrial and space-based RF transceiver platforms [1], [2]. However, to facilitate their deployment, high-performing and highly miniaturized RF filters would need to be integrated in their RF front-ends to suppress spurious signals from the active stages (e.g., amplifiers) as well as the interference from other satellite and military applications that operate at neighboring frequencies and degrade the quality-of-service (QoS) [2], [3].

Several RF bandpass filter (BPF) configurations have been presented in the open technical literature to date for *K*-/*Ka*-band applications [3]–[14]. They include planar-based architectures using compound metal oxide semiconductors (CMOS) [4], gallium arsenide (GaAs), and silicon germanium (SiGe) technologies [5], as well as polymer-on-glass-based configurations [6], [7]. 3-D integrated architectures using substrate integrated waveguides (SIWs) and air-filled cavities have also been reported to improve insertion loss (IL) at the expense of size. In [6], a 3rd order SIW-BPF using slot-type resonators on low temperature co-fired ceramics (LTCCs) is discussed. It exhibits a center frequency of 40 GHz with an IL of 1.4 dB and a fractional bandwidth (FBW) of 10.2%. *Ka*-band SIW BPFs are also reported in [8]–[11] using dielectric-filled [9], [11] and air-filled [8] SIWs. 3-D high-quality factor (Q) air-filled BPFs using SU-8 coaxial resonators and silicon-based resonators are discussed in [12]–[14] having low levels of IL between 0.5 and 0.8 dB, however, they are large in size and cannot be easily integrated with other IC components.

Substrate integrated coaxial (SIC)-resonator-based BPFs [15], [16] have been extensively investigated as technology alternative to SIW due to their small size while exhibiting moderate Q. However, the majority of them have been implemented for low frequencies (<7 GHz). Si-based air-field coaxial BPFs have been implemented at higher frequencies (20–40 GHz) with relatively high-Q [14]. Nevertheless, they are large and complex to manufacture due to the need for multiple microfabrication-based processing steps. Furthermore, they require multi-part assembly that needs post-fabrication tuning.

In this letter, a new approach to materialize low loss and compact quasi-elliptic BPFs using glass-integrated SIC resonators and mixed electromagnetic (EM) couplings that create transmission zeros (TZs) without the need for cross couplings is reported. The organization of this letter is as follows. In Section II, the filter concept is presented. The practical implementation of these filters using a glass platform and their experimental testing is reported in Section III. Lastly, Section IV outlines the contributions of this work.

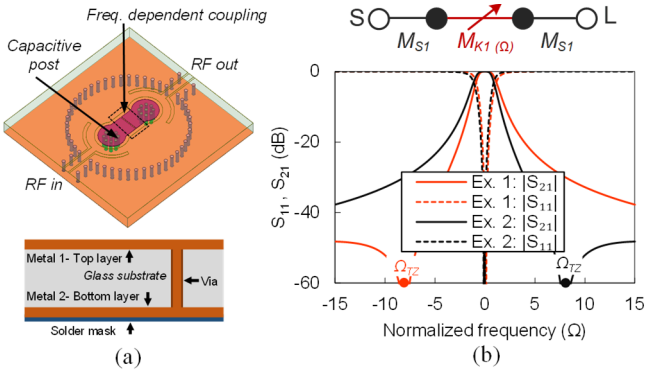

(a) (b)

Fig. 1. (a) Three-dimensional EM simulation model of the two-pole/one-TZ SIC BPF shaped by two EM-coupled coaxial posts and side view of the glass-integration stack-up: glass substrate is 400 μm, metal 1, 2 are 10 μm thick and the solder mask is 14 μm. (b) CRD of a two-pole/one-TZ BPF. White circles: non-resonating nodes, black circles: resonating nodes, black-line: frequency-independent coupling elements, red line: frequency-dependent coupling that creates one TZ in the out-of-band response. Synthesized S-parameters using the following coupling coefficients: example 1: $M_{S1} = 0.841$, $M_{K1} = 0.707 + 0.088\ \Omega$, example 2: $M_{S1} = 0.841$, $M_{K1} = 0.707 - 0.088\ \Omega$.

II. Theoretical Foundations

The details of the SIC glass-based BPF concept are depicted in Fig. 1 through its 3-D EM model, corresponding coupling routing diagram (CRD) and CRD-synthesized responses. As shown in Fig. 1(b), a two-pole/one TZ transfer function is obtained by only using two resonators (black circles) and incorporating a frequency-dependent inter-resonator coupling element (red line representing the inverter M_{K1}) within a two-resonator configuration. The TZ is obtained at a frequency Ω_{TZ}, where $M_{K1}(\Omega_{TZ}) = 0$ and can be placed below or above the BPF passband by readily changing the sign of $M_{K1}(\Omega) = M_0 + M_1 \cdot \Omega$ where M_0 is the inter-resonator coupling at the center frequency of the passband and M_1 is the coupling slope with respect to the normalized frequency Ω. Two

Manuscript received November 28, 2021; revised April 1, 2022; accepted April 10, 2022. Date of publication April 13, 2022; date of current version May 25, 2022. Recommended for publication by Associate Editor P. Chahal upon evaluation of reviewers' comments. *(Corresponding author: Dimitra Psychogiou.)*

Dimitra Psychogiou is with the School of Engineering, University College Cork, Cork, T12 K8AF Ireland, and also with the Tyndall National Institute, Cork, T12 R5CP Ireland (e-mail: dpsychogiou@ucc.ie).

Andrea Ashley is with the Department of Electrical, Computer, and Energy Engineering, University of Colorado Boulder, Boulder, CO 80309 USA (e-mail: andrea.ashley@colorado.edu).

Color versions of one or more figures in this article are available at https://doi.org/10.1109/TCPMT.2022.3167270.

Digital Object Identifier 10.1109/TCPMT.2022.3167270

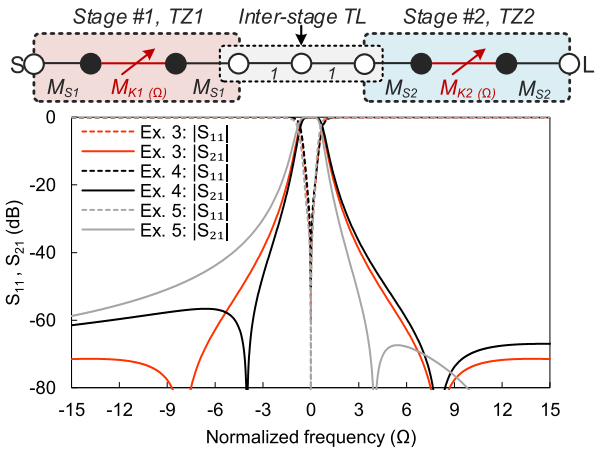

Fig. 2. CRD of a two-stage four-pole/two-TZ BPF comprising two stages that are cascaded with an inter-stage TL. The figure also provides example synthesized S-parameters using the following couplings (obtained by optimization): example 3: $M_{S1} = 0.841$, $M_{K1} = 0.707 - 0.088$ Ω, $M_{S2} = 0.841$, $M_{K2} = 0.707 + 0.088$ Ω, example 4: $M_{S1} = 0.841$, $M_{K1} = 0.707 - 0.088$ Ω, $M_{S2} = 0.841$, $M_{K2} = 0.707 + 0.1768$ Ω, example 5: $M_{S1} = 0.841$, $M_{K1} = 0.707 - 0.0589$ Ω, $M_{S2} = 0.841$, $M_{K2} = 0.707 - 0.1768$ Ω.

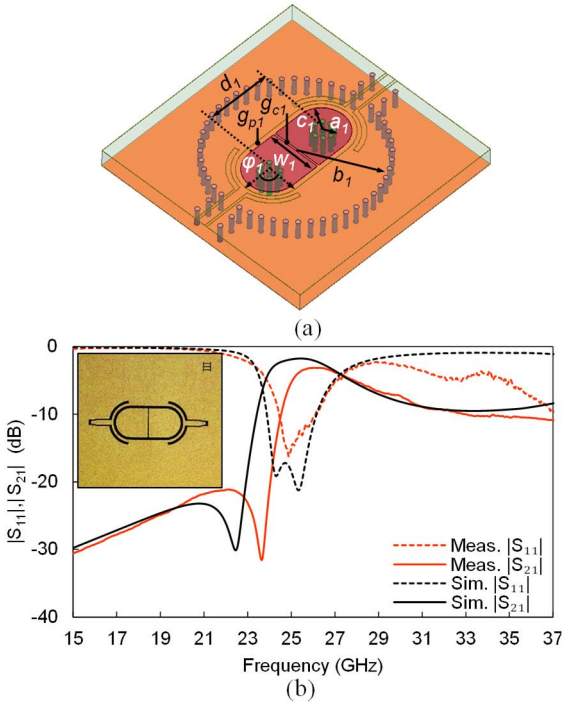

Fig. 3. Two-pole/one-TZ SIC BPF. (a) Three-dimensional simulation model having the following geometrical dimensions: $b_1 = 1.6$ mm, $w_1 = 1.1$ mm, $a_1 = 0.2$ mm, $c_1 = 0.55$ mm, $g_{c1} = 0.038$ mm, $g_{p1} = 0.1$ mm, $\varphi_1 = 73°$, $h = 0.4$ mm, $d_1 = 0.55$ mm. (b) EM-simulated and RF-measured response of the manufactured prototype that is provided in the inset of this figure.

example synthesized responses of the two-pole/one-TZ BPF concept are provided in Fig. 1(b) for alternative M_{K1}parameters (obtained by optimization of the CRD values in MATLAB) that are used to demonstrate TZ control. As shown, the roll-off sharpness and out-of-band rejection can be increased with the aid of the frequency-dependent coupling. This is advantageous when implementing the filter as cross couplings are no longer needed.

The practical implementation of the two-pole/one-TZ CRD is performed using a double-resonant SIC resonator [16], [17] implemented by a glass-filled cylindrical cavity with radius b_1 (created by an array of Cu-filled vias that connect the top and bottom metallization, the via spacing is between 0.12 and 0.23 mm) and two capacitively loaded

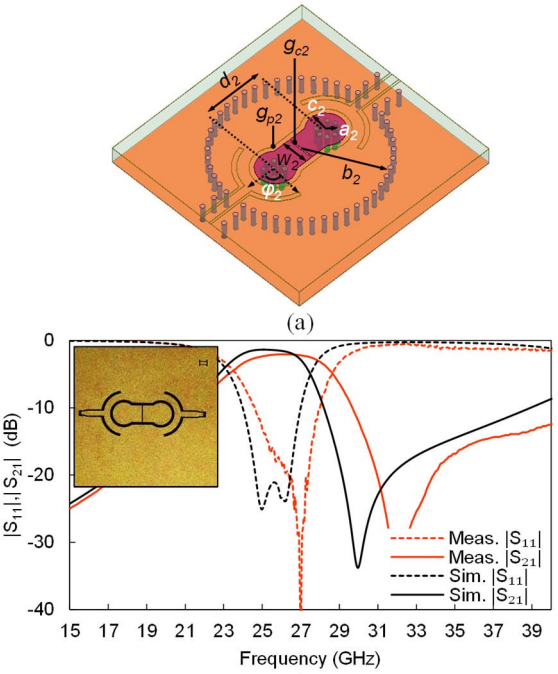

Fig. 4. Two-pole/one-TZ SIC BPF. (a) Three-dimensional simulation model having the following geometrical dimensions: $b_2 = 1.75$ mm, $w_2 = 0.6$ mm, $a_2 = 0.2$ mm, $c_2 = 0.4$ mm, $g_{c2} = 0.03$ mm, $g_{p2} = 0.1$ mm, $\varphi_2 = 70°$, $h = 0.4$ mm, $d_2 = 1.4$ mm. (b) EM-simulated and RF-measured response of the manufactured prototype that is provided in the inset of this figure.

metallic (geometrical details are provided in Fig. 3) posts. The posts are shaped by Cu-filled vias that are arranged in a cylindrical shape with radius a_1. The capacitive loading of the posts is performed by adding a circular metal piece (radius C_1) at the top end of the post and by introducing a capacitive gap g_{p1}. A mixed EM coupling is created by: 1) the distance d_1 of the capacitive posts (magnetic coupling) and 2) the size of the inter-post section (electric coupling) that has a width W_1 and a capacitive gap g_{c1} to materialize the frequency-dependent inverter of the CRD M_{K1}. The external coupling elements (admittance inverters M_{S1}) are materialized with slot openings with radius φ_1 at the upper metallization layer and bring the RF signal within the cavity.

Higher-order transfer functions comprising higher number of poles and TZs can be readily created by cascading multiple two-pole/one TZ stages through inter-stage transmission lines (TLs). This is shown in Fig. 2 for the example case of a four-pole/two TZ BPF that is shaped by two in-series cascaded stages (stages 1 and 2). Example synthesized transfer functions are also provided in the same figure using the CRD values in the caption. As shown, quasi-elliptic BPF profiles can be obtained by readily adjusting the location of the TZs. This is achieved by changing the magnitude and sign of the frequency-dependent coupling elements M_{K1} and M_{K2} that allow the TZs to be placed symmetrically or asymmetrically around the passband.

III. Experimental Validation

Three SIC filter prototypes were designed, manufactured, and tested at *K*-/*Ka*-band to practically validate the SIC BPF concept. They include: 1) a two-pole/one TZ BPF with a TZ below the passband; 2) a two-pole/one TZ BPF with a TZ above the passband; and 3) a four-pole/2 TZ BPF. All of the BPFs were implemented in a high-frequency glass-based stack up [see Fig. 1(a)] that comprises of: 1) two 10-μm thick metallization layers and Cu-plated via holes; 2) a 14-μm solder mask layer (not used); and 3) a 400 μm thick glass substrate with dielectric permittivity $\varepsilon_r = 6.4$ and tan$\delta = 0.01$. The

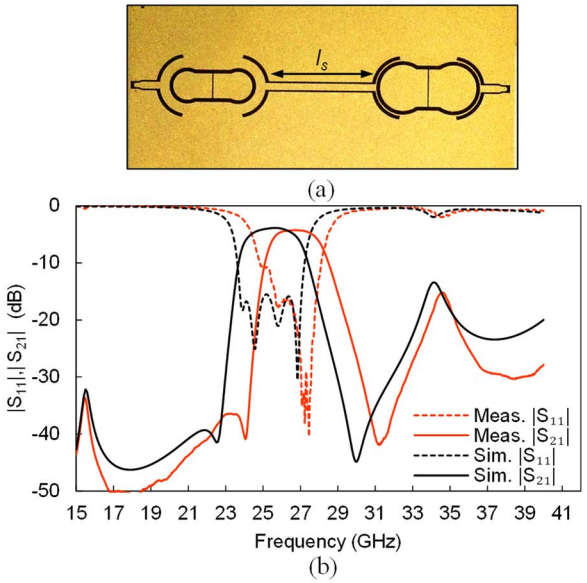

Fig. 5. (a) Manufactured prototype of the two-stage SIC BPF with l_s = 2.96 mm. (b) EM-simulated and RF-measured response of the two-stage SIC BPF prototype.

TABLE I
COMPARISON WITH SOA *K*-/*Ka*-BAND BPFS

Ref.	[4]	[5]	[6]	[8]	[11]	[13]	T.W
f_{cen} (GHz)	25	28.4	40	33	28.5	36	26.7
IL (dB)	2.5	1.8	1.4	1	1.6	0.5	4.5*
FBW (%)	31	11	10.2	10.1	7	4.5	10.9
N	2P/2TZ	2P/3TZ	3P	4P	5P	2P	4P/2TZ
Size (mm^2)	0.48	0.18	5.3	50	132	72	37
Tech.	CMOS Planar	GaAs Planar	LTCC 3D	SIW 3D	Silica 3D	Si 3D	Glass 3D

N: number of poles (P)/ transmission zeros (TZs), * including the loss of the GSG pad to GCPW transition

filters were designed in ANSYS HFSS using the design guidelines in Section II and conventional filter design methodologies that allow to translate a CRD to a physical structure as for example the ones in [14]–[16]. RF testing was performed through GSG 150 μm probes and a Keysight N5224A power network analyzer.

Fig. 3 illustrates the manufactured prototype and RF measured response of the two-pole/one TZ BPF with one TZ placed below the passband. It exhibits the following characteristics: passband centered at 26.7 GHz, minimum in-band IL of 3 dB, FBW of 11%, and a TZ located at 23.6 GHz. Its corresponding EM simulated response is also shown in the same figure alongside the EM model [see Fig. 3(b)] of the filter. They appear to be in a fair agreement. The observed frequency shift is due to the manufacturing tolerances, however, it is only 3.8%. Similarly, Fig. 4 depicts the manufactured prototype and RF measured response of the two-pole/one-TZ SIC BPF with one TZ placed above the passband and exhibits the following transfer function characteristics: passband centered at 26 GHz, IL of 2 dB, FBW of 21%, and a TZ at 32 GHz. The high-order SIC four-pole/two TZ prototype and its corresponding RF measured response is provided in Fig. 5. It exhibits a passband at 26.7 GHz, IL of 4.5 dB, FBW of 11%, and two TZs at 24 and 31.3 GHz. Its EM simulated response is also depicted in the same figure and appears to be in a fair agreement. A comparison of the SIC glass-integrated concept with other State of the art (SOA) planar and 3-D BPFs is provided in Table I. As shown, the SIC concept exhibits smaller size than most of the 3-D integration concepts. Whereas it has higher IL than the BPF in [6], it allows for TZs to be obtained in its out-of-band response without the need to increase the filter volume or the use of cross-couplings.

IV. CONCLUSION

A class of SIC BPFs have been presented for communication applications in the *K*-/*Ka*-bands. The letter studied the potential of a high-frequency glass-based integration concept for the realization of highly miniaturized quasi-elliptic BPFs using cascaded two-post SIC cavity resonators. The operating principles of the SIC BPF concept were validated experimentally through the manufacturing and testing of three BPF prototypes in the *K*-/*Ka*-band.

REFERENCES

[1] P. Wang, J. Zhang, X. Zhang, Z. Yan, B. G. Evans, and W. Wang, "Convergence of satellite and terrestrial networks: A comprehensive survey," *IEEE Access*, vol. 8, pp. 5550–5588, 2020.

[2] V. Deslandes, J. Tronc, and A.-L. Beylot, "Analysis of interference issues in integrated satellite and terrestrial mobile systems," in *Proc. 5th Adv. Satell. Multimedia Syst. Conf., 11th Signal Process. Space Commun. Workshop*, Sep. 2010, pp. 256–261.

[3] P. Matthews, "Approaching the 5G mmWave filter challenge," *Microw. J.*, May 2019. [Online]. Available: https://www.microwavejournal.com/articles/32228-approaching-the-5g-mmwave-filter-challenge/

[4] C.-L. Yang, S.-Y. Shu, and Y.-C. Chiang, "Design of a K-band chip filter with three tunable transmission zeros using a standard 0.13-μm CMOS technology," *IEEE Trans. Circuits Syst. II, Exp. Briefs*, vol. 57, no. 7, pp. 522–526, Jul. 2010.

[5] G. Shen, W. Che, W. Feng, Y. Shi, and Y. Shen, "Low insertion-loss MMIC bandpass filter using lumped-distributed parameters for 5G millimeter-wave application," *IEEE Trans. Compon., Packag., Manuf. Technol.*, vol. 11, no. 1, pp. 98–108, Jan. 2021.

[6] S. W. Wong, R. S. Chen, K. Wang, Z.-N. Chen, and Q.-X. Chu, "U-shape slots structure on substrate integrated waveguide for 40-GHz bandpass filter using LTCC technology," *IEEE Trans. Compon., Packag., Manuf. Technol.*, vol. 5, no. 1, pp. 128–134, Jan. 2015.

[7] X.-P. Chen and K. Wu, "Self-packaged millimeter-wave substrate integrated waveguide filter with asymmetric frequency response," *IEEE Trans. Compon., Packag., Manuf. Technol.*, vol. 2, no. 5, pp. 775–782, May 2012.

[8] F. Parment, A. Ghiotto, T. P. Vuong, J. M. Duchamp, and K. Wu, "Ka-band compact and high-performance bandpass filter based on multilayer air-filled SIW," *Electron. Lett.*, vol. 53, no. 7, pp. 486–488, Mar. 2017.

[9] M. Ali, K.-Q. Huang, M. Swaminathan, P. M. Raj, and R. R. Tummala, "Laminated glass-based, compact inline stepped-impedance resonator bandpass filters for 5G new radio modules," *IEEE Trans. Compon., Packag, Manuf. Technol.*, vol. 11, no. 4, pp. 708–711, Apr. 2021.

[10] M. Ali, A. Watanabe, T. Kakutani, P. M. Raj, R. R. Tummala, and M. Swaminathan, "Heterogeneous integration of 5G and millimeter-wave diplexers with 3D glass substrates," in *Proc. IEEE 70th Electron. Compon. Technol. Conf. (ECTC)*, Jun. 2020, pp. 1376–1382.

[11] Y. Uemichi *et al.*, "Narrow-band and low-loss bandpass filter for 5G built of silica-based post-wall waveguide," in *Proc. 50th Eur. Microw. Conf. (EuMC)*, Utrecht, The Netherlands, Jan. 2021, pp. 559–562.

[12] A. Jaimes-Vera, I. Llamas-Garro, M. Ke, Y. Wang, M. J. Lancaster, and L. Pradell, "Polymer-based micromachined rectangular coaxial filters for millimeter-wave applications," *Int. J. Microw. Wireless Techn.*, vol. 3, no. 2, pp. 1790–1803, Apr. 2011.

[13] Y. Tian, H. Wang, K. Lee, and K. Ang, "On-chip air-gapped cavity resonators and filters for mm-wave IC applications," *IEEE Trans. Compon., Packag.,s Manuf. Technol.*, vol. 6, no. 10, pp. 1549–1554, Oct. 2016.

[14] Z. Yang, D. Psychogiou, and D. Peroulis, "Design and optimization of tunable silicon-integrated evanescent-mode bandpass filters," *IEEE Trans. Microw. Theory Techn.*, vol. 66, no. 4, pp. 115–120, Apr. 2018.

[15] M. D. Hickle and D. Peroulis, "Tunable constant-bandwidth substrate-integrated bandstop filters," *IEEE Trans. Microw. Theory Techn.*, vol. 66, no. 1, pp. 157–169, Jan. 2018.

[16] D. Psychogiou and R. Gomez-Garcia, "Quasi-absorptive substrate integrated bandpass filters using capacitively-loaded coaxial resonators," in *IEEE MTT-S Int. Microw. Symp. Dig.*, Los Angeles, CA, USA, Aug. 2020, pp. 663–666.

[17] D. Psychogiou and R. Gomez-Garcia, "Compact substrate-integrated bandstop filters using double-resonant coaxial resonators," *IEEE Microw. Wireless Compon. Lett.*, vol. 30, no. 10, pp. 941–944, Oct. 2020.